Post-print: Langmans, J., Roels, S. (2015). Experimental analysis of cavity ventilation behind rainscreen cladding systems: A comparison of four measuring techniques. *Building and Environment, 87* (5), 177-192.

Experimental analysis of cavity ventilation behind rainscreen cladding systems: a comparison of four measuring techniques

Jelle Langmans*, Staf Roels

Department of Civil Engineering, Building Physics Section, University of Leuven
Kasteelpark Arenberg 40 - bus 02447, BE-3001 Heverlee, Belgium

** Corresponding author. Tel: +32 16 321348; fax: + 32 16 32 19 80.*
E-mail address: jelle.langmans@bwk.kuleuven.be (J. Langmans)

Abstract

The present article elaborates on the comparison of four measuring techniques quantifying the ventilation rate behind typical cladding systems in wall elements. In total eight full-scale test walls have been investigated in a test building located in a maritime temperate climate (Belgium). Two different commonly used cladding systems are studied: (a) brick veneer and (b) fibre cement sidings. The test walls were installed on the Southwest and Northeast façades of the building corresponding to the orientations with most extreme exposure regarding solar radiation, wind directions and wind-driven rain. In total four different measurement techniques to quantify the ventilation rate in these systems have been applied: a) tracer gas techniques, b) indirect method based on pressure measurements, c) direct method based on anemometers and d) method based temperature and relative humidity registration. The results indicate that the ventilation rate behind vented brick veneer is two orders of magnitude lower than behind ventilated cladding systems with sidings. It was found that the most appropriate measuring technique of a wall system is depending on the ventilation rate, and hence on the type of cladding. For brick veneer claddings, the method deriving the air flow rate from the pressure gauges was found to be most suitable. In the wall systems with sidings, on the other hand, the ventilation rates were sufficiently high to be measured accurately with the anemometers.

Keywords: Cavity ventilation, field tests, measuring techniques, airflow, brick veneer, sidings

NOMENCLATURE

Roman

A	Area	(m^2)	θ	Temperature	(°C)
ACH	Air change rate	(1/h)	δ_a	Vapour permeability of stagnant air (kg/s/m/Pa)	
C	Sampling concentration	(mg/s)			
C_d	Discharge coefficient	(-)	**Abbreviations**		
C_p	Pressure coefficient	(-)			
D	Dosing rate	(mg/s)	OHJ	Open head joint	
d_h	Hydraulic diameter	(m)	EIFS	Exterior Insulation Finishing System	
f	friction factor	(-)			
h	Height	(m)	**Subscripts**		
Q	Air flow rate	(m^3/s)	a	air	
T	Temperature	(K)	ex	exit	
u	velocity	(m/s)	ent	entrance	
R	specific gas constant	(J/kg/K)	c	cavity	
Re	Reynolds number	(-)	tur	turbulent flow	
P	Pressure	(Pa)	trans	transitional flow	
RH	Relative humidity	(%)	lam	laminar flow	
t	time	(s)	m	average (in space)	
V	Volume	(m^3)	out	outdoor	
Sh	Sherwood number	(-)	buoy	buoyancy	
			v	vapour	

Greek

β	vapour transfer coefficient	(s/m)
ϵ	surface roughness	(m)
ξ	loss factor	(-)
λ	friction factor	(-)
ρ	density	(kg/m^3)

1. Introduction

Moisture is one of the key elements affecting the durability and performance of building enclosures. Among others, ventilated rainscreen cladding is a typical measure to improve the moisture safety of building envelopes [1]. Cladding systems serve as a capillary break and drainage plane between the exterior climate and the inner group of structural elements. In addition, ventilated rainscreen cladding enhances the removal of excessive moisture by means of ventilation. While gravity-driven drainage of rain water is a well-understood process to avoid water penetration, the convective evacuation of moisture is a complex process related to the configuration of the cavity, the hygrothermal properties of the construction materials and the climatic conditions. As a consequence this topic has been investigated by several authors for various claddings systems and different methods. A great number of studies have focussed on the drying efficiency of cavity ventilation. Both experimentally [2-6] and with numerical HAM modelling techniques [7-12] the interaction of the ventilation rates on the hygrothermal performance have been investigated. An important uncertainty in these studies is related to the assumed ventilation rate. For example in the experimental study of Schumacher [2,5], climate chamber tests have been performed in which a constant air change rate was varied between 5-40 ACH in different test runs. In the hygrothermal simulation study of Salonvaara et al. [10] and the work of Künzel et al.

[12], on the other hand, a constant ventilation rate between 1.5-150 ACH and a constant ventilation rate of 50 ACH respectively, were assumed. The conclusions in the abovementioned studies are highly related to the presumed ventilation rates. Because the estimated ventilation rates significantly differ between some of these studies, the outcome is not always conclusive and in a few cases even contradictive [13].

A straightforward way to tackle this issue in future studies is collecting more accurate data on the actual ventilation rate behind cladding systems. In the international literature we can distinguish between three main methodologies applied to quantify ventilation rates. A first group corresponds to numerical studies in which CFD[1]-software is used [e.g. 14-16]. These numerical models allow selecting specific meteorological conditions to verify the air flow pattern behind cladding systems. For example, while Labat et al. [16] focuses on solar driven air flow behind open joint claddings, Nore et al. [14] studied the impact of wind-driven cavity ventilation behind sidings. A second group consists of methods in which the cavity flow conditions are modelled by hydraulic networks [e.g. 17-18]. These models typically link a driving force model for thermal buoyancy and wind pressures differentials based on theoretical pressure coefficients (Cp) with a resistance network to model the airflow in the cavity. The final group of methods is related to studies in which the cavity ventilation is measured on *in-situ* walls [e.g. 3,20-21].

The present article focusses on this last group of experimental methodologies. Several measuring techniques in which the air change rate is measured directly or indirectly have been discussed in the literature. A common strategy is the application of tracer gas methods. Gudum [3] studied the air change rate behind a plexiglass cladding material in field conditions by injecting nitrous oxide with a constant dose. Bassett and McNeil [21], similarly, measured the cavity ventilation rate with a continuous emission carbon dioxide tracer method for brick veneer cladding, sidings and EIFS. They concluded that this method is applicable for a wide range of cavity ventilation rates (over three orders of magnitude). An indirect measuring protocol was developed by TenWolde et al. [23] who measured air pressure differences between the top and bottom vents of wall cavities with vinyl sidings and calculated the corresponding ventilation rates using airtightness measurements on these systems. In addition, cavity ventilation behind cladding systems has also been measured on a number of configurations with anemometry [e.g. 3,23]. A very detailed study was performed by Falk and Sandin [23] who studied cavity ventilation by measuring the air velocity in the middle of the cavity with an omnidirectional anemometer. The authors derived in this study a method to quantify the driving potentials related to thermal buoyancy and wind differential pressures. Based on this method they proposed a method to compensate for the constantly changing flow direction in the cavity as a results of the highly unstable nature of wind, which could not be detected by the

[1] Computational Fluid Dynamics

omnidirectional anemometer. Finally, also smoke visualisation methods are discussed in the literature. For example in Sweden, the air change rate behind brick veneer cladding with and without open head joints have been estimated with this method [23]. Apart from estimating the air change rate behind brick veneer, the authors obtained interesting observations regarding the instability of the air flow patterns.

The abovementioned previous field measurements documented a wide range of techniques to quantify cavity ventilation rates. However, only a few of these works investigated the accuracy of these methods. Moreover, these tests have been performed on a diversity of cladding systems and materials ranging from very limited ventilation rates (brick veneer) to highly open systems (open joints sidings) impeding a direct intercomparison between the different existing studies.

The aim of the present work is to conduct detailed field measurements in which all of the abovementioned methods will be compared on the same wall configuration. Two different cladding systems have been selected (brick veneer and fibre cement sidings) to allow comparing these methods for various levels of cavity ventilation. In addition a new method to derive the ventilation rate based on the measured humidity levels within the cavity will be proposed, so, in total four different techniques will be compared:

- Tracer gas measurements
- Air velocity measurements with hot bead anemometry
- Pressure differential measurements combined with hydraulic network
- Novel method based on measured temperature and relative humidity profiles

The aim of the present article is to compare the applicability of these measuring techniques to quantify cavity ventilation. First the reader will be introduced to the test-setup, sensor positions and an exploratory investigation of the air flow patterns with smoke injection. Thereafter, in the subsequent sections, each measuring technique and the corresponding results will be discussed individually. Finally the different methods will be compared and their applicability will be outlined in the discussion section at the end of the article.

2. Field tests

2.1. Test-setup and wall configurations

In-situ measurements have been conducted at the VLIET-test building located in Leuven, Belgium (50°52'N, 4°41'E). This test building has a rectangular plan with the measuring sections located in the longitudinal façades, oriented to the Northeast and the Southwest. In Belgium, Southwest is the direction of prevailing winds, wind-driven rains and solar irradiation. Northeast oriented façades, on the other hand, hardly receive any sun or rain. This single storey test building is partly constructed with duo-pitched roofs and partly with a flat roof. The

building has one weather station located above the ridge of the sloped roofs module and one in the nearby free field, both at 10 m above ground level. They register the outside climate parameters on a 1-minute basis (temperature, humidity, wind speed and direction, global solar irradiation, horizontal rainfall). For more information on the building's geometry, location and orientation the reader is referred to [25-27]. In total eight separate full-scale test walls (2.7 x 1 m²) were installed in the flat-roof module of the test building (see Figure 1). Two test walls with brick veneer cladding and two walls with fibre cement sidings are oriented both to the Northeast and to the Southwest direction.

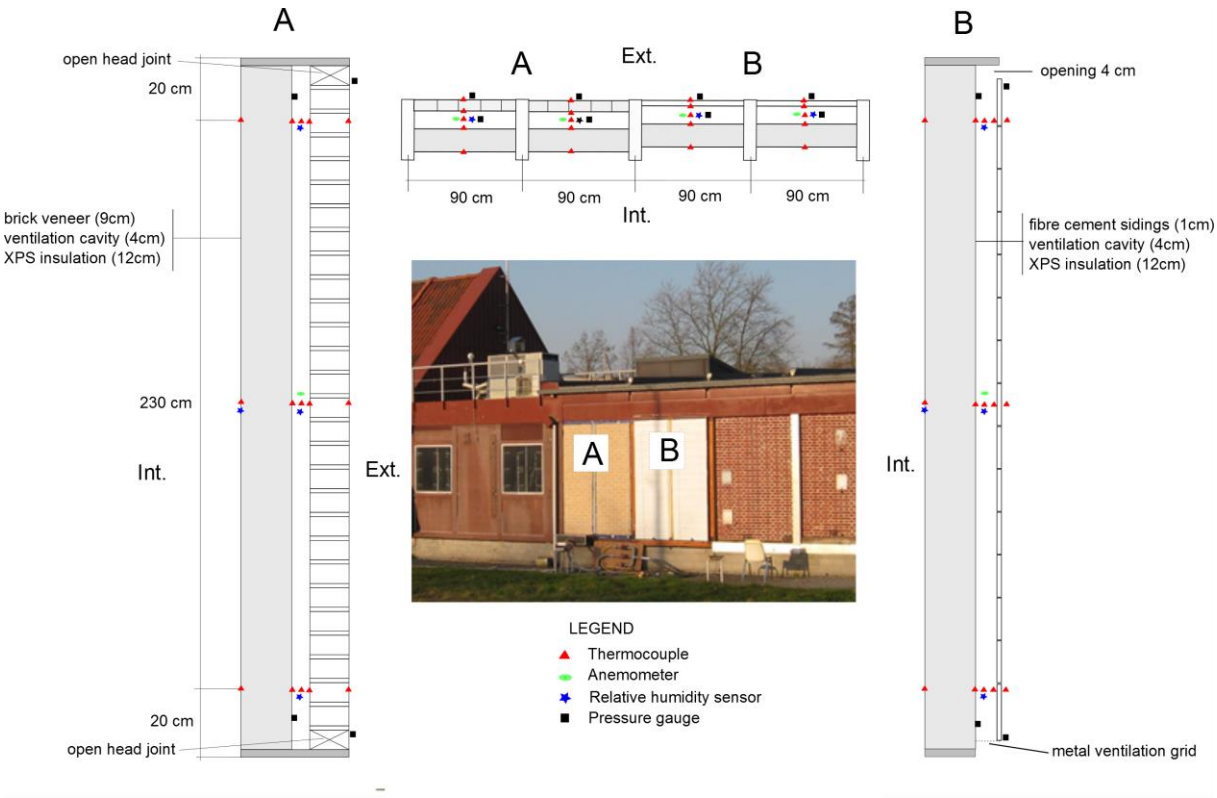

Figure 1: Southwest façade of the VLIET test building with (A) brick veneer test wall and (B) test wall with fibre cement sidings.

The overall configuration of the test walls is presented in Figure 1. Standard brick veneer of 9 cm is applied in which a grid system is installed at the top and bottom to allow a variation in the number of open head joints. In this way the number of open head joints can be varied from zero to 30 openings per meter with the size of each opening being 3.5x1.5x9 cm³. For the other test walls white coloured water repellent fibre cement sidings with a thickness of 1cm are applied. These test walls have an opening of 4 cm at the top and are provided with a metal grid to protect the wall from vermin at the bottom. The cavity depth of all test walls was 4 cm and at the inside a thermal, vapour and airtight break was applied (an XPS insulation panel of 12 cm thick). To limit the heat and moisture transport from the interior climate (19 °C/50 %RH) and between adjacent cavities, each wall was carefully caulked at the inside and an XPS-layer of 5 cm was provided between each test wall. Also the edges of

the brick veneer layer and the sidings have been precisely sealed to avoid air leakages at those points and to promote two-dimensional conditions in the air cavities.

2.2. Sensor positioning and accuracy

Several measuring strategies to register the air change rates within the cavities have been applied. First a comprehensive data logging system was established to allow continuous measurements. Each test wall is provided with 15 thermocouples, 4 relative humidity sensors and 1 hot bead anemometer (CTA), covering the most important positions in the ventilation cavity. The sensors are distributed in three rows: 20 cm from the bottom, at middle height and 20 cm from the top and are placed in the middle of the wall section. Figures 1 depicts an overview of the sensor positions as placed within each wall section. In addition, each test section is provided with three pressure gauges (differential pressure transmitters [37]) to measure to pressure drop across the top and bottom open head joints and the pressure differential across the overall cavity. Here, special attention was given to install the ends of the pressure tapes perpendicular to the walls.

To increase the accuracy of the measurements, the complete set of thermocouples and humidity sensors installed in the data logging system have been calibrated beforehand. With a sensor specific calibration, the accuracy of reading could be increased compared to the global sensor accuracy given by the manufacturer. In this way it is possible to compensate for errors such as the cold junction temperature and the position of the connection. The thermocouples and relative humidity sensors have been calibrated with an optical dew point transmitter with an accuracy of +/-0.1 °C on the global temperature and +/-0.2 °C on the dew point temperature. The thermocouples were calibrated at four temperatures (1, 10, 20 and 25 °C) and the humidity sensors at three humidity levels (30, 80 and 99 % RH). Table 1 summarizes the applied sensors with the corresponding accuracies and measuring range.

Sensor	Manufacturer	Type	Accuracy	Range
Thermocouple	Thermo Electric	type TT	± 0.1 °C	-20/60 °C
RH-sensor	Honeywell	HIH-4000/21	± 2 %	0/100 %
Pressure gauge	Halstrup Walcher	P26 and P92	± 0.3 Pa	± 50 Pa
Hot bead anemometer	Sensor-Electronic	AirDistSys 5000F	± 0.02 m/s or 1% of reading	0.05-5 m/s
Tracer gas equipment	Brüel & Kjaer Innova	type 1303	± 2 %	/

Table 1. Accuracy and measuring range of applied sensors.

In addition to the continuous logging system, the necessary equipment was installed to allow periodical SF_6-tracer gas analysis measurements. One of the test sections oriented to the Northeast was provided with 5 sample tubes distributed across the height of the cavity and one dosing tube at mid-height.

3. Exploratory smoke visualisation tests

Before the actual tests took place, smoke visualisation tests have been performed to obtain qualitative information on the air flow patterns behind the different cladding systems. For this analysis the insulation panels have been replaced by transparent plexiglass boards to allow the visualisation of smoke injected in the cavity. Two configurations have been tested: ventilation cavity with fibre cement sidings and brick veneer cladding with two open head joints at the top and bottom. Smoke was injected from the inside at the bottom of the Southwest oriented cavities with a smoke pencil producing white smoke. The tests have been performed on December 12th (average outside temperature 5.9 °C and wind velocity during the test below 1 m/s).

A major difference was noticed between the air flow patterns of the two test walls. For the wall with sidings the injected smoke plume reached the top of the cavity much faster (10-12 seconds) than for the brick veneer (25-40 seconds). The tests on the walls with sidings revealed that the rising smoke remained compact and indicated that the velocity was more or less the same across the width of the cavity. In contrast, the smoke plume behind the brick veneer cladding distributed across the cavity. In addition, the velocity was not constant across the width of the cavity. Higher speeds were noticed close to the open head joints at the lower parts of the cavity. In higher regions of the cavity this profile disappeared, but even then, no constant velocity was reached across the width.

Though previous studies (e.g. Sandin [23]) have documented air change rates based on similar smoke injection tests, the authors of the article at hand stress the inaccuracy of this method for three reasons: a) replacing the inner group of materials by plexiglass to visualise the smoke influences the driving potentials, b) at low air change rates the smoke distributes across the cavity, impeding its localisation and c) the smoke is injected at a different temperature influencing the flow pattern. Therefore this method is not included in the present work as a measuring method.

4. Tracer gas measurements

Two different tracer gas techniques have been applied. In the first test series the air change rate was derived from a constant dosage test. Thereafter the cavity ventilation was deduced based on the decay method.

4.1. Constant dosage

0n 12/12/2013, a tracer gas campaign with a constant dosage within one of the Northeast oriented brick veneer test walls has been performed. The experiment consisted of three steps: a) openings closed, b) all openings opened (30 openings) and c) one ventilation opening at the top and one at the bottom. During the experiment a constant dosage of 1.5 mg/s was injected in the middle of the air cavity and the disturbed SF_6-tracer gas was

sampled at five locations across the height of the cavity. Figure 2 shows the measuring results for these three test steps together with the wind speed and wind direction during the experiment.

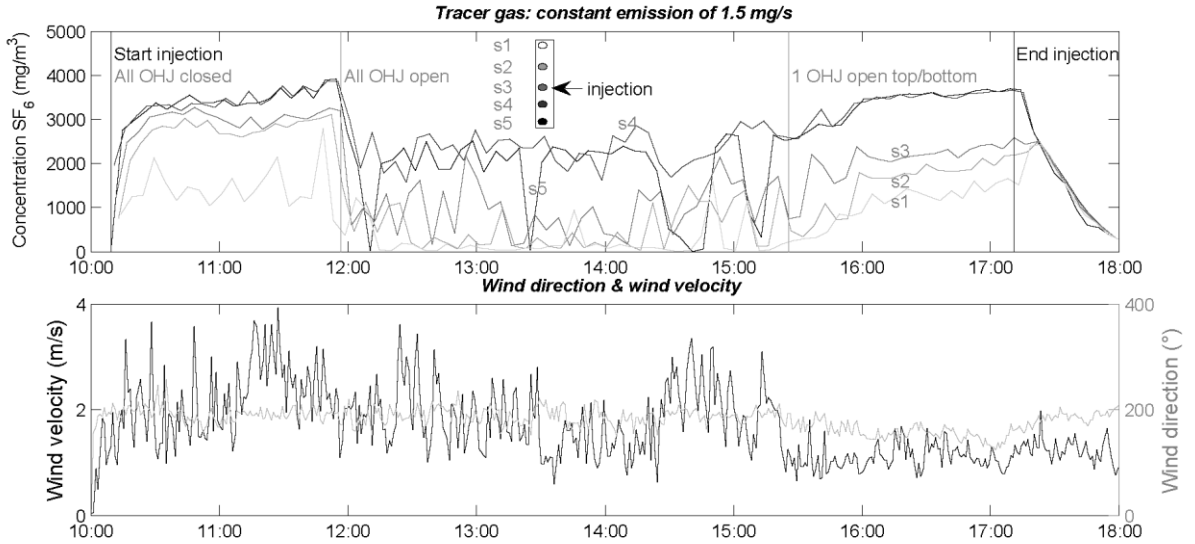

Figure 2: Tracer gas experiment on 12/12/2013 for Northeast-oriented brick veneer cladding: top) sampling concentration across height of the cavity and bottom) corresponding wind speed and wind direction (North=0°, South=180°) during the experiment.

Theoretically, for well-mixed volumes, the air flow rate can be derived based on the dosed and sampled tracer gas concentration by:

$$ACH = 3600.\frac{D}{C_{aver}}.\frac{1}{V_{cav}} \quad (1)$$

in which D is the dosing rate (1.5 mg/s for this instance), C_{aver} is the averaged sampled concentration (mg/m³) and V_{cav} is the cavity's volume (m³).

Table 2 provides the averaged (in space and time) concentrations of all sampling points within the cavity and the corresponding calculated air change rate. In addition this table includes in grey the minimum and maximum in time averaged values.

	Closed vents	All vents open	1 vent open
Concentration (SF_6) mg/m³	1378/ 2845/ 3503	198/ 1180/ 2339	1096/ 2268/ 3346
ACH (1/h) (Eqn.1)	36/ 18/ 14	253/ 42/ 22	46/ 22/ 15

Table 2: Averaged sampled concentration and calculated air change rate (minimum/averaged/maximum)

Figure 2 and table 2 indicate large variations between the different measuring points, with higher tracer gas concentration at the bottom sampling points. This is related to poor mixing of the air in the cavity which consequently results to a large spread in the calculated air change rates.

The same measuring method with constant dosage was repeated on 10/06/2013 for one of the Southwest oriented walls with sidings with free top and bottom ventilation opening. The concentrations SF_6 in this test run were fluctuating between 500 and 3500 mg/m³ and again the concentration was higher at the bottom and lower at the top. However, the differences of the concentrations across the height were smaller than in the test with brick veneer cladding. The resulting averaged ventilation rate calculated with Eqn. 1 from combining all sampling points during this period was 183 1/h. The calculated ventilation rate based on the upper sampling point corresponded to 287 1/h and at the bottom sampling point to 118 1/h. The smaller range between the minimum and maximum can be explained by the higher mixing process as a result of higher ventilation rates behind the sidings in comparison with the brick veneer. Even with all ventilation holes opened, the ventilation rate behind the brick veneer was smaller because of the lower driving potential during this test. Although, the wind speed was moderate during both tests (fluctuating between 1-4 m/s), the sidings which were oriented to the Southwest and tested in summer received more solar radiation than the brick veneer walls which were tested on the North East side and in winter.

In addition it should be noted that the applied SF_6 gas is significantly heavier than ambient air. For cladding systems corresponding to low ventilation rates - or in periods with low driving potentials - the tracer gas drops down after injection. In that case the higher density of SF_6 corresponds to a higher downward driving potential and thus a biased air flow rate. This should be taken into account when comparing the tracer gas method with other methods.

4.2. Decay method

In a second tracer gas experiment a certain concentration of SF_6 was realised within the cavity whereafter the injection was stopped. The ventilation rate can then be derived from the decay of the concentration. Figure 3a zooms in on a period measured on the brick veneer straight after the constant dosage test (section 4.1). The decay can be modelled with the following equation according to [35,p192]:

$$V\frac{dC_i}{dt} + Q.C_i = D \quad \text{with} \quad \boldsymbol{C_{i(t)}} = \boldsymbol{C_{i(0)}} e^{-\frac{Q}{t}} \tag{2}$$

where Q is the air flow rate (m³/s), D is the tracer gas dosing rate (mg/s) and t is time (s). Figure 3 illustrates the tracer gas decay at the end of the measurement and gives in addition the modelled fit according to Eqn. 2 for an air change rates between 1 and 10 ACH. The figures indicate that the actual ventilation rate lies within this order of magnitude.

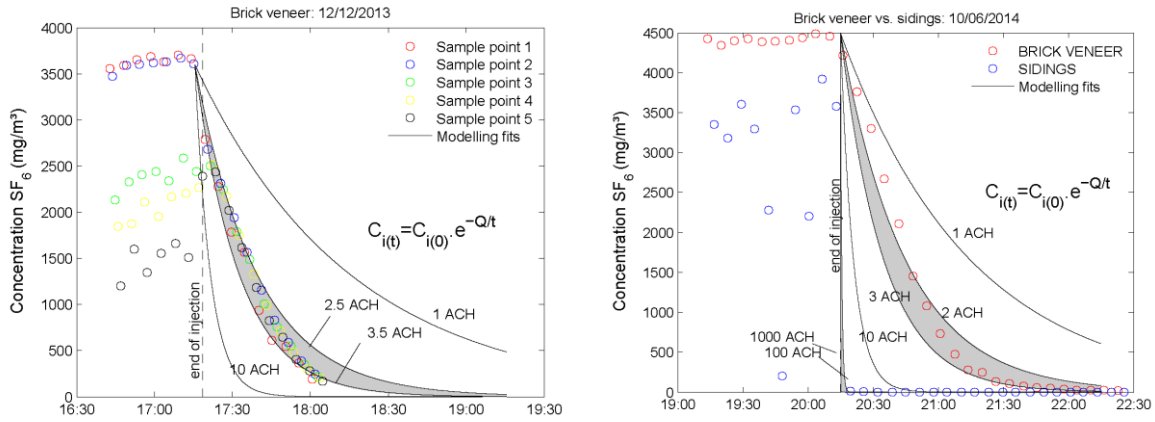

Figure 3 : Measured tracer gas decay and modelling fit.

This decay experiment was repeated in June 2014 for a Southwest oriented cladding system with sidings and brick veneer. These results are presented in Figure 3b in which the same order of magnitude for the air change behind the brick veneer was found. The ventilation rate behind the sidings is however at least one order of magnitude larger. Because of the low frequency of measuring points related to this technique it is only possible to conclude that the air change rate behind the sidings is larger than 100 ACH. Consequently, it should be concluded that the tracer gas technique in which the decay of tracer gas is registered is only applicable to estimate the air changes levels below 100 ACH with the measuring frequency of the applied equipment.

As for the constant dosage tracer gas experiment, it should be noted that the higher density of the SF_6 gas influences the derived ventilation rate. This complicates a direct comparison of the tracer gas method with the other measuring techniques.

5. Indirect method: pressure differential measurements

This section derives a method to determine the air change rate from the measured pressure differential across the cladding. First, the method will be illustrated for brick veneer cladding. In section 7.2 this method will be briefly repeated for its application on the walls with sidings.

Ventilation cavities can be modelled as a hydraulic network characterised by a unique relation between the total air pressure differential ΔP_{driv} across the cavity and the resulting airflow (Q). This relation can be applied to deduce the ventilation rate indirectly from the measured air pressure differentials across the cavity. The position and type of pressure gauge sensors used have already been introduced in section 2.1. This section elaborates on how the relation between the air pressure differential and the corresponding ventilation rate for the brick veneer cavity of this study was determined both theoretically and experimentally.

5.1. Theoretical determination of the ACH(ΔP)-curve

This section derives the theoretical relation between the pressure differential and air flow rate based on the assumption that the cavity can be modelled as a continuous hydraulic network. This methodology, applying the well-established Darcy-Weisbach friction formula, has been used by several authors to model air flows in building components [e.g. 23, 29-30]. This steady-state method basically divides the problem in a sequence of air resistances. Imposing a global driving pressure across the system results in a pressure drop caused by friction across each separate resistance. For the configuration of a typical brick veneer cladding this system can be subdivided in five consecutive resistance elements; 1) entrance (open head joint), 2) bend, 3) air channel, 4) bend, and 5) exit (open head joint):

$$\Delta P_{driv}=\Psi.\frac{\rho_a.Q^2}{2} \quad ,\Psi=\mathrm{f}.\frac{h}{d_h}.\left(\frac{1}{A_c}\right)^2+\xi_{ent}.\left(\frac{1}{A_{en}}\right)^2+\xi_{ex}.\left(\frac{1}{A_{ex}}\right)^2+2.\xi_{bend}.\left(\frac{1}{A_c}\right)^2 \qquad (3)$$

in which ΔP_{driv} (Pa) corresponds to the total pressure across the cavity, Q is the resulting air flow rate (m³/s) and Ψ combines the geometrical and fluid mechanical properties of the separate air flow resistances. Herein *h* corresponds to the height (m) of the cavity, *f* is the friction factor, d_h is the hydraulic diameter, ξ are the loss factors of the entrance, exit and the bends and *A* is the area of the cavity (*c*), entrance (*ent*) and exit (*ex*) respectively.

First, the friction losses of the cavity itself can be modelled as a rectangular duct of which the flow characteristics are widely available in the literature [e.g.31-32]. The resistance of such parallel ducts are formulated as a function of its geometry and flow regime (Re-number). In the present article the friction losses presented by Kronvall [32] are adopted (see Table 3).

Parameter	**Equation**
Hydraulic diameter d_H	$d_h=\frac{2.d.w}{d+w}$
Friction factor f_{lam} (Re≤2300)	$\frac{64}{[\frac{2}{3}+\frac{11}{24}.\frac{d}{w}\left(2-\frac{d}{w}\right).Re]}$
Friction factor f_{trans} (2300 ≤ Re ≤ 2300)	$\frac{(3500-Re)\lambda^{Re=2300}+(Re-2300).\lambda^{Re=3500}}{1200}$
Friction factor f_{tur} (Re ≥ 3500)	$[2.\log(\frac{-4.793}{Re}.\log\left(\frac{10}{Re}+0.2.\frac{\varepsilon}{d_h}\right)+0.2698.\frac{\varepsilon}{d_h})]$

Table 3: Equations for determination of the hydraulic diameter and friction factors (f) [32].

The entrance and exit loss factors for the configuration of this study, on the other hand, are very specific to ventilated brick veneer cladding. Consequently they are not available in the international literature. To the authors knowledge only Straube and Burnett [33] elaborated on the air resistance of open head joints in brick veneer. In a laboratory investigation the characteristics of several types of vents and open head joints have been measured. The open head joints measured by Straube and Burnett [33] which are approaching most closely the configuration of this study were 6.5x1x9 cm³. Straube and Burnett express the air flow through the open head joint by means of the general power law formulation:

$$Q = C_d . A_{OHJ} . \Delta P^n \tag{4}$$

in which C_d = 0.626 m³/Pa^{n-1}/s corresponds to the discharge coefficient, A_{OHJ} = 6.5x1 cm² to the area of the open head joint and n = 0.555 (-) to the flow exponent. Combining Eqn. 3 and 4, the local loss factor of the open head joints can be expressed as:

$$\xi_{OHJ} = \xi_{ent} = \xi_{ex} = \frac{2}{\rho_a . C_d^2 . \Delta P^{(2n-1)}} \tag{5}$$

Which is presented in Figure 4 as a function of the air velocity $u_{m,OHJ}$.

The third loss factor corresponds to the bends at the top and bottom of the cavity where the air flow direction changes. These type of standard configurations have been measured by several authors [e.g. 23,31, 32]. In this paper the experimental data of Falk and Sandin [23] is applied in which the relation between the loss factor and averaged velocity is given by:

$$\xi_{bend} = 1.8 - 0.3 . u_m \tag{6}$$

represented in Figure 4 below.

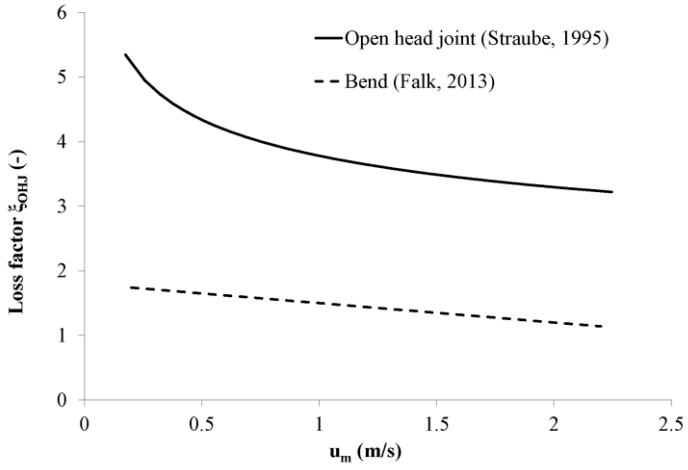

Figure 4: Loss factor for bend [23] and open head joint [33].

The global air flow characteristics of the brick veneer cladding can be derived by combining all friction losses (Eqn. 5). Herein, the friction losses for the top and bottom open head joint are equal (continuous line, Figure 4) as well as the losses related to the upper and lower bend (dashed line, Figure 4). The characteristics of the parallel duct are adopted from Table 3. It should be stressed that the air permeance of the brick veneer cladding itself is neglected in the overall cavity system. The resulting relation between the air flow in the cavity and the pressure differential across the top and bottom openings is compared with the experimentally derived relation in Figure 6 of section 5.3.

5.2. Experimental determination of the ACH(ΔP)-curve

In addition to the abovementioned theoretical derivation, a direct pressurisation test was performed to determine the airflow characteristics of the brick veneer cladding system on site. The aim of this additional test is to verify the justification of the theoretical hydraulic model with the inherent assumption that the permeability of the brick veneer can be neglected herein.

At the bottom of the brick veneer test wall, a manifold was tightened with closed-cell EPDM of 0.5 cm to the ventilation grid to create a negative pressure across the open head joints by means of an air pump (see Figure 5). By stepwise increasing the pressure difference across the air cavity and measuring the air flow rate and associated pressure difference across the specimen a data set was obtained, which was curve fitted with a power law relation:

$$Q_a = a\Delta P_{box}^b \tag{7}$$

where Q_a (m^3/ h) refers to the airflow rate, ΔP_{box} (Pa) stands for the pressure difference across the manifold, a (m^3/(Pa)) is the air permeance coefficient and b (-) the air permeance exponent of the system. The flow rate Q_a was measured with a turbine flowmeter (Trigas FI) measuring in a range from 3.4 m^3/h to 36 m^3/h with an accuracy of 0.6 %. The air pressure differential between the manifold and the outdoor climate was measured with a pressure sensor (4 DG-700) with an accuracy of 1 %. In addition, also the pressure drops across the top and bottom ventilation holes and the total pressure differential across the brick veneer cavity are measured with the sensors discussed in section 2. The pressurisation tests have been performed for the situation with one open head joint at the top and bottom. In a second step the test was repeated after sealing the top ventilation opening. In the following section these experimental results are compared with the theoretically derived curve from section 5.1.

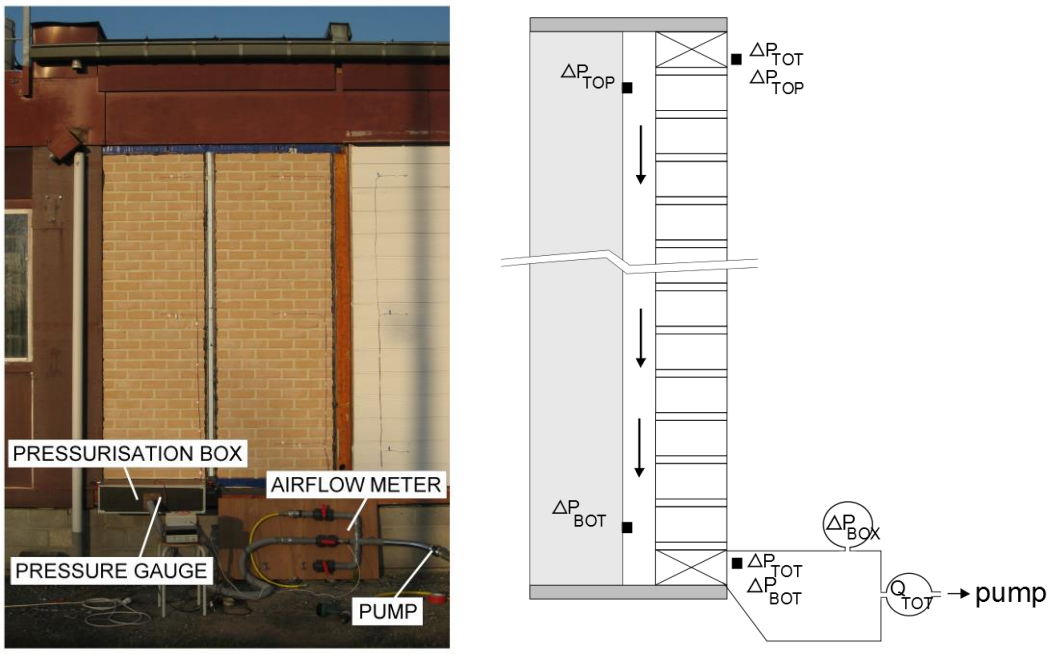

Figure 5: Picture and schematic overview of the test-setup for brick veneer cladding system.

5.3. Comparison between theoretical hydraulic network and pressurization test

This section compares the airflow characteristics of the brick veneer cladding obtained by the experimental procedure (section 5.3) with the theoretical concept of a hydraulic network (section 5.1). Figure 6a gives the air change rate (1/h) as a function of the total air pressure differential across the cavity. The dots and squares in this figure correspond to the experimental data for the situation in which the open head joint at the top was open and sealed respectively. The red curves in this figure correspond to the values predicted by the hydraulic network approach for the same two configurations. This figure illustrates that assuming the air permeance of the brick veneer negligible in the overall system does not hold. According to the hydraulic model the airflow remains zero for the configuration without a top ventilation hole. The experimental data indicates, on the other hand, a significant air flow for this composition (squares). The same phenomenon is observed in Figure 6b in which the red curve corresponds to the calculated pressure drop across top and bottom vent. The experimental data in this figure, in contrast, registered a lower pressure drop across the top vent and a higher pressure loss at the bottom ventilation hole. This again proves the existence of an air flow through the brick veneer layer.

In summary the comparison between the continuous hydraulic network and the experimental data indicates that the air permeance of the brick work cannot be neglected. Therefore the network was extended with the air flow resistance of bricks. The air permeability of brick veneer was adopted from Hens [34] who measured half-stone thick veneer with massive bricks (19x9.5x4.5 cm) and 10 mm wide mortar joints. Hens [34] fitted the obtained data with the power law (Eqn. 7) for which he obtained $a=34.8.10^{-6}$ (kg/m²sPa) b=0.81 (-). This function can be

transformed to express the friction loss through the brickwork:

$$\xi_{brick} = \frac{2.\rho_a}{a^2 \Delta P^{(2b-1)}} \quad (8)$$

By including the air resistance of the brick veneer layer the network becomes a parallel circuit of series connection of resistances instead of a continuous path. The dashed lines in Figure 6 correspond to the air flow characteristics predicted by the network including the air permeance of brick veneer. The figure indicates that taking the bricks permeability into account in the model results in a far better agreement with the experimental data. As a consequence, this relation (dashed lines in Figure 6) will be applied in the remainder of this paper for the calculation of the air change rate based on the continuous air pressure measurements.

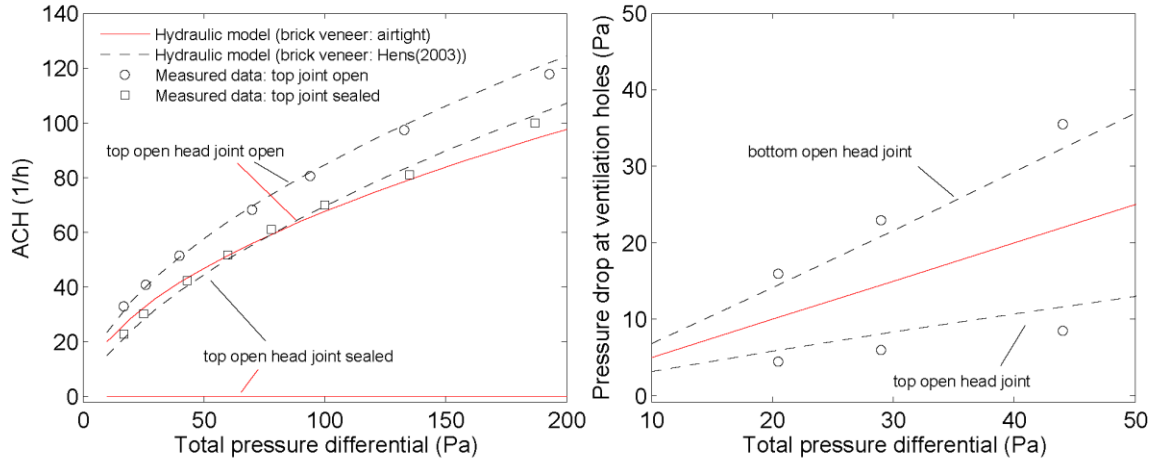

Figure 6: A) Measured and calculated ACH(ΔP)-curve for situation with and without sealing the top ventilation hole and B) Pressure drop across top and bottom ventilation holes as a function of the global air pressure differential across the cavity.

6. Direct method: anemometer measurements

The test walls are provided with omnidirectional hot bead anemometers in the middle of the ventilation cavities (see Figure 1) registrating the air velocity every 10 s. For fully-developed laminar flow conditions between plan parallel walls the shape of the velocity profile corresponds to a parabolic function, so, the ratio between the maximum velocity (u_{max}) and averaged velocity (u_m) is 2/3 [29]. This straightforward relation does not hold for higher air velocities. Experimental work by Falk and Sandin [23, Figure 7], however, showed that this ratio lies between 0.61 and 0.69 for Reynolds numbers below 5700 for similar shaped ventilation cavities. Because this corresponds to a small deviation from the parabolic velocity profile, the air change rates (ACH (1/h)) in the present work are calculated with a ratio of 2/3:

$$ACH = \frac{u_{max}.2/3}{h}.3600 = \frac{u_m}{h}.3600 \quad (9)$$

with h the height of the cavity. The advantage of this direct measuring method with anemometers is its possibility to perform a prompt and continuous registration of the air change rate. The major disadvantages on the other hand are the lower limit of these sensors (u_{max} > 0.05 m/s or ACH > 45 1/h), their independency of the flow direction and the low spatial measuring resolution (local one point measurement).

7. Comparison of direct and indirect measuring technique

This section discusses the results of both the direct and indirect measuring method. First, the measuring results will be compared for brick veneer cladding (section 7.1). Thereafter the analysis is conducted for the walls with sidings (section 7.2).

7.1. Brick veneer cladding

Two different continuous measurement techniques to quantify the ventilation rates have been introduced: a) direct measurements with a~~n~~ thermo-anemometer (section 6) and b) indirect measurements by means of treating the brick veneer cladding as a hydraulic network and registering the pressure difference across the cavity (section 5). This section compares both measuring approaches for the first week of February 2014. The comparison is conducted for one of the Southwest oriented test walls with brick veneer. The first three graphs in Figure 7 contain climatic information and the actual comparison of the measured air change rate with both techniques is illustrated in the last two graphs of Figure 7.

Figure 7a gives the measured wind direction and wind speed in the field near the test building on a minutely basis. The wind is predominately blowing from the Southwest (225°) during the measuring span and combines both calm days (e.g. 03/02) and days with strong wind (07/02). Figure 7b provides the measured total air

pressure differential across the cavity on hourly averaged basis (right axis). This figure, in addition, differentiates between the air pressures induced by wind and those driven by temperature differences between the cavity and the outdoor air. For the first, both hourly (right axis, full lines) and 1-minutely (left axis, grey dots) data is provided. The latter is more stable and is therefore only given on hourly basis. It should be stressed that the wind induced air pressures (black curve) are compensated for the temperature differences between outside and inside air. The tube of the upper pressure tap runs to the pressure gauge at the floor level inside the test building which is conditioned at 18°C. The pressure tap at the bottom of the cavity, however, is directly connected to the pressure gauge without a difference in altitude. Density differences induced by the temperature variations between the inside and ambient air, introduce a static air pressure differential ($\Delta P_{tube,pos}$) for which the wind induced air pressure differential (ΔP_{wind}) should be compensated:

$$\Delta P_{wind} = \Delta P_{meas} - \Delta P_{tube,pos} = \Delta P_{meas} - (\rho_{outdoor} - \rho_{indoor}).h.g \quad (10)$$

in which ρ is the air density of the indoor and outdoor air, h is the height of the cavity and g is gravimetrical force.

The second potential for cavity ventilation is related to temperature differences between the air cavity and the outdoor climate. The corresponding buoyancy induced air pressure differentials, calculated based on the measured outdoor temperature and the temperature in the middle of the air cavity according to Eqn. 11, are included in Figure 7b in red:

$$\Delta P_{buoy} = 3462 \left[\frac{1}{T_{out}} - \frac{1}{T_{cm}}\right].h \quad (11)$$

In which T_{out} (K) corresponds to the outdoor air and T_{cm} (K) to the temperature in the cavity (averaged across the height). Figure 7c shows the measured temperatures: (a) air temperature in the middle of the cavity (black), (b) the indoor (red) and outdoor (blue) temperature and (c) the outside surface temperature of the brick veneer (grey). During the first days of the experiment (02/02 – 05/02) sunny periods increased the air cavity temperature up to 15-18 °C while for the other days the cavity temperature followed the outer temperature more closely. In addition, this figure shows a phase shift between the surface temperature of the brick and the air temperature of the cavity due to thermal inertia of the cladding.

The comparison between the abovementioned two continuous measuring techniques is concentrated in Figure 7d and 7e. The first graph presents the calculated air change rate based on the measured pressure differential across the cavity. As the pressure differences in Figure 7b are highly fluctuating, the air flow direction is constantly changing (grey dots). Positive values in the graph correspond to an overpressure at the top of the cavity, and thus, a downward air flow. The one-minutely data on Figure 7d (grey dots, left axis) shows air change rates up to

40 1/h for this measuring span. Much lower air change rates (<10 1/h) are obtained when the data is hourly averaged (right axis, black curve). In addition, the uncertainty due to the accuracy of the pressure gauge is included in Figure 7d. Due to the non-linear relation between the pressure and the corresponding cavity ventilation (Figure 6 and 9) the errors are higher at low wind speeds. This will be discussed more in detail in section 7.2. Figure 7e provides the air change rates obtained from the direct air velocity measurements. Because the air velocities are measured with an omnidirectional anemometer, they do not contain any information on the flow direction. The measured air velocities are transformed in Figure 7e to the corresponding air change rates

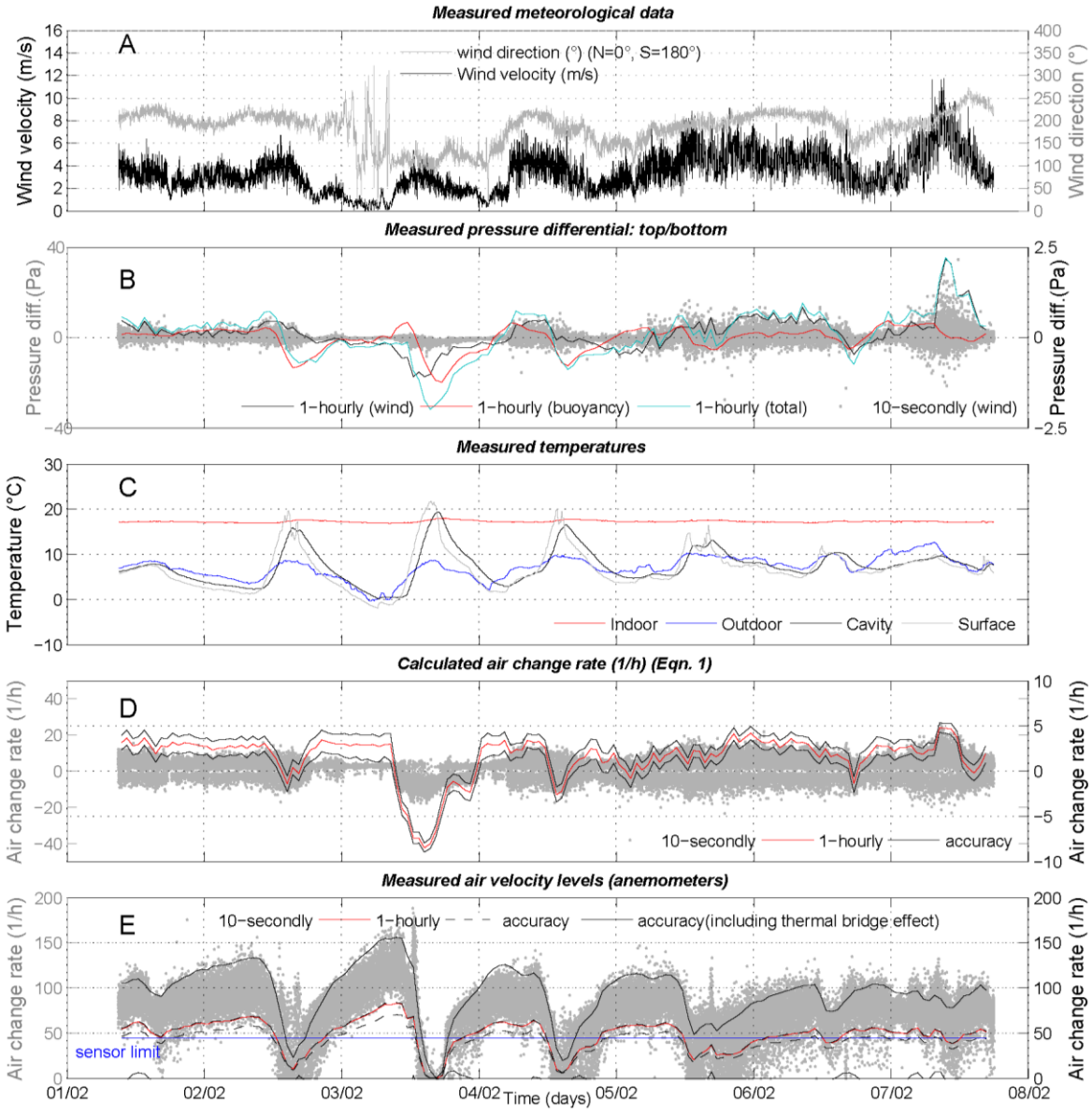

Figure 7: Brick veneer wall (Southwest façade) A) Wind velocity and direction, B) measured pressure differential, C) measured temperatures, D) air change rates in the cavity (based on pressures gauges) and E) air change rates (based on anemometers).

with Eqn. 9. In addition, this figure provides the uncertainty on the results due to the sensor accuracy and the error related to the position of the anemometer (dashed line) which will be discussed more in detail in section 7.2.

In most of the measuring period the measured air velocities are exceeding the lower accuracy limit provided by the manufacturer which is indicated in blue (0.05 m/s or 45 1/h for the current configuration). Yet figure d and e show that the results from the direct and indirect method are not in agreement which each other. As will be explained below this is caused by the inaccuracy of the direct method in this range of air changes rates. Figure 8 reveals that the air change rates directly measured with the anemometers correlate to the temperature difference across the insulation layer instead. Further investigations in which an additional anemometer had been installed from the outside through the brick veneer leaf revealed that the anemometer measurements from the inside were biased by local buoyancy driven air flows around the sensor. These local air flows were induced by the thermal bridging effect of the metal anemometer through the insulation layer. Based on this observations it should be concluded that the air flow in the cavity behind the brick veneer is too low to overrule local air movements around the sensors induced by thermal bridging effects. The errors related to this thermal bridge effect are included in Figure 7e (black lines) which reveals that this direct measuring method is invalid for the determination of air change rates in this range. As a consequence a comparison between the direct and indirect method for brick veneer becomes irrelevant.

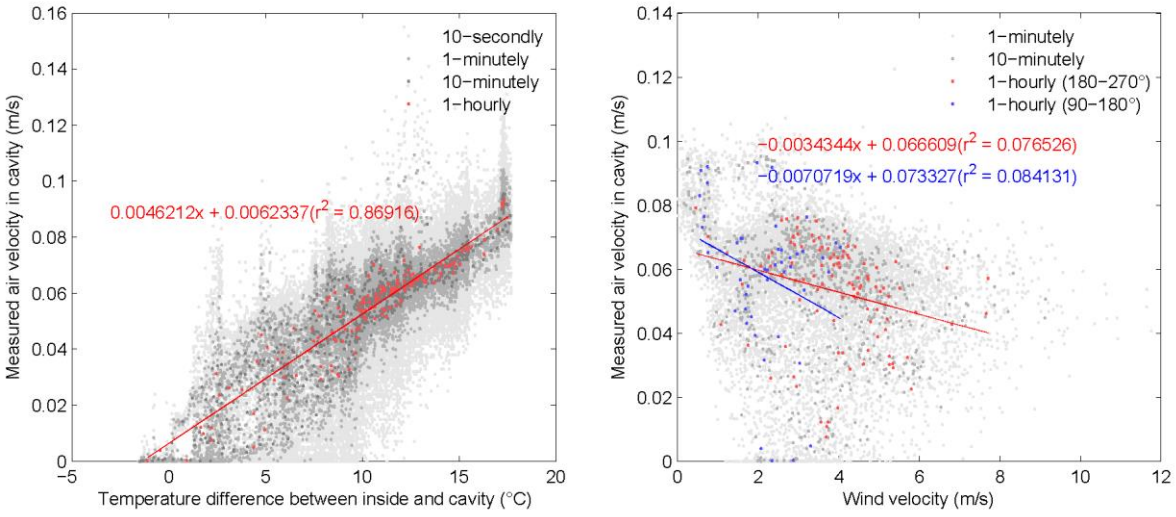

Figure 8: Measured air velocity in cavity as a function of temperature difference between the cavity and the inner climate (left) wind velocity (right) of brick veneer cladding oriented to Southwest façade.

7.2. Comparison of direct and indirect measuring technique – Sidings

ACH(ΔP)-curve

The methodology discussed in section 5.1 is applied to define the hydraulic network of the cladding systems with sidings. Figure 1 showed that the ventilation cavity is open at the top and is provided with a metal ventilation grid at the bottom. Consequently the network consists of 4 air flow resistances: (1) bend (top), (2) cavity, (3) sidings, (4) bottom (bend), bottom (ventilation grid). For the top and bottom bend the relation expressed in Eqn. 4 and illustrated in Figure 4 is applied. The resistance of the cavity itself is again based on the work of [31], given in Table 3. The permeability of the sidings and the metal ventilation grid at the bottom was measured with the test-setup discussed in [35]. This apparatus is designed to quantify the air flow resistance of specimen of 35 cm by 35 cm. The sidings which had a width of 20 cm were cut to specimen of 17.5 cm by 35 cm, so, one joint of 35 cm could be measured. The metal grid – with a width of 4 cm – was connected to a plexiglass board to allow its installation in the existing test rig. Both specimens were curve fitted to the power law of Eqn. (2). For the metal grid this resulted in a C_d-coefficient of 0.018 $m^3/ Pa^{n-1}/s$ and a flow exponent n of 0.5 (-). The sidings corresponded to a C_d-coefficient of 0.004 $m^3/m^2/Pa^{n-1}/s$ and a flow exponent n of 0.59. These relations were transformed with Eqn. 8 to friction loss factors from which the global air flow characteristics of the overall ventilation cavity was derived according to method discussed in section 5 assuming a parallel network of series connections. Figure 9 provides an overview of the total air flow characteristics of both the brick veneer cladding (left axis, black) and the walls with sidings (right axis, grey). First an error analysis on the direct and indirect method will be provided. Thereafter, both measuring methodologies will be compared for sidings.

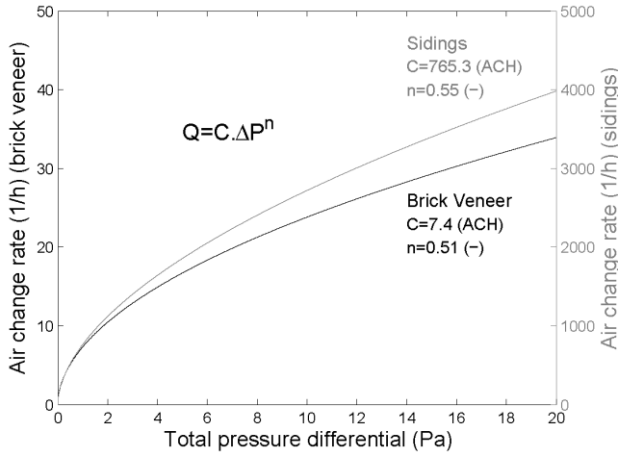

Figure 9: Air flow characterists of the cladding systems investigated as a function of the total air pressure differential across the cladding.

Error analysis

Section 7.1 already briefly touched the errors related to both measuring techniques based on the results of brick veneer cladding. Yet this section revealed that the direct measuring method is not capable of measuring in the low range of air change rates related to brick veneer (<100ACH). This section will discuss the errors related to both methods in detail to allow a comparison in the following section.

In what follows only the first error is taken into account which can be divided into the sensor accuracy and the error related to positioning the pressure tubes. As great care was given the installation of the pressure taps (see section 2), the latter is neglected here. Table 1 showed that the accuracy of the pressure measurements is 0.15 Pa in a range of +/-50Pa. Figure 10 (left) illustrates its impact on the predicted air change rate based on the relation given in section 7.2. The figure shows that the air change rate obtained for the siding system based on the indirect method is highly uncertain once below 300 1/h.

The right graph in Figure 10 illustrates the errors related to the direct method with anemometers on the other hand. Here we distinguish four errors: measuring range of the sensor (>0.05m/s), accuracy of the sensor (1% of reading), error related to the position of the anemometer in the cavity and the error due to the cold bridge effect of the anemometer (see section 7.1, Figure 8). The first two errors are straightforward. The third expresses the error induced when the anemometer is not exactly positioned in the middle of the cavity. As discussed in section 6 a parabolic profile with the maximum in the middle of the cavity is assumed to derive the averaged velocity (in space). In the present analysis an uncertainty of +/- 1 cm on the position of the sensor is put forward. Note that this error can only underestimate the actual air change rate. Finally, the last error is related to the cold bridge effect of the anemometer which occurs in periods with a high temperature difference between the inside and the cavity. In what follows the relation given in Figure 8 (left) is applied to calculate this error. Yet in Figure 10 this error is illustrated for a temperature difference of 20°C which corresponds to an error of 89 1/h.

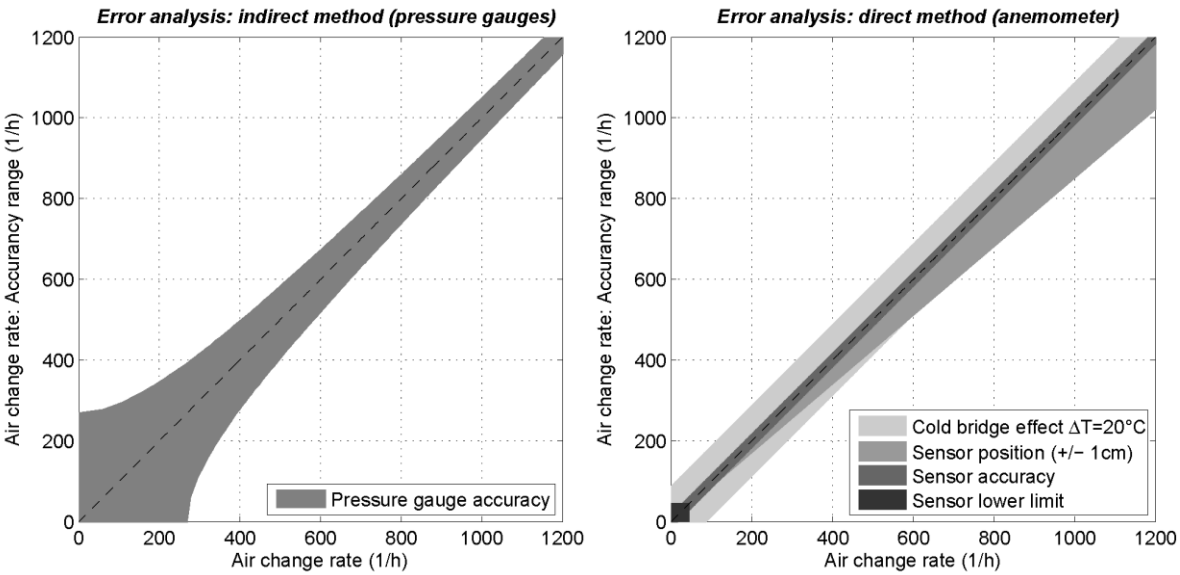

Figure 10: Accuracy of air change rate measured with the indirect method with pressure gauges (left) and direct method with anemometers (right).

Results

In similarity with section 7.1, Figure 11 provides the measured temperatures and the air change rates derived from both (a) the measured pressure differentials (b) and the measured point velocities. Compared to the brick veneer cladding the cavity's peak air temperature (black) is lower and has no phase change with the outer temperature (blue). The air change rate profiles calculated from the measured velocities (Figure 11c) are in line with the ones derived from the measured pressure differential (Figure 11b). Where the latter can distinguish between upward (negative) and downward (positive) flow, the former only registers unidirectional flow conditions. The pressure measurements indicate that the air flow rate is changing direction with a high frequency. Consequently, a direct quantitative comparison between both methods is difficult. The air change rate derived from the measured velocity in the cavity overestimates the actual rate. Because of the high frequency in direction changes the air might not always be removed from the cavity at low air flow rates. The applied anemometer, which does not register the direction of the velocity, can not compensate for this overestimation. On the other hand the hourly averaged air change rates based on the pressure differentials (black line, Figure 11c) will underestimate the actual air flow rate for the opposite reason. For example, imagine that the absolute pressure differential remains the same for one hour. When the pressure would be negative the first 30 minutes and positive the next 30 minutes, the hourly averaged air change rate would be zero. This issue is addressed more in detail below in Figure 12 where the direct method is compared to the indirect method.

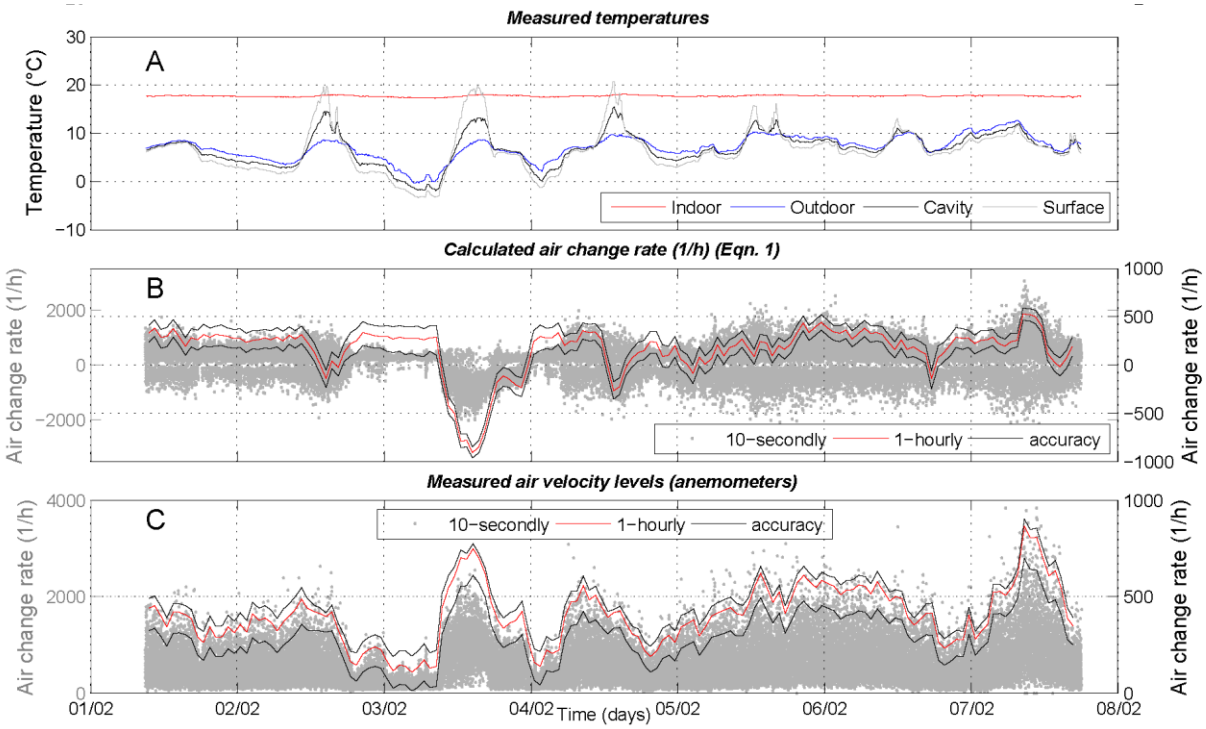

Figure 11: Wall with sidings system (Southwest façade) : A) measured temperatures, B) calculated air velocity levels in the cavity and C) measured air velocity level (anemometer).

This issue of the overestimation of the anemometer results was already addressed by Falk and Sandin [23]. They derived for predominant upward flow conditions (sunny periods with low wind velocities) an overestimation ratio of the air change rate based on anemometer measurements of 5 to 40 %. The applicability of their proposed value is verified in Figure 12 in which both measuring techniques are directly compared for the data of February. Figure 12d presents the air change rate based on (a) the measured velocity (black), (b) absolute hourly averaged pressure difference (blue), (c) hourly averaged absolute pressure differential and (d) velocity measurements reduced by 5-40% based on the findings of Falk and Sandin [23] (grey surface). In addition Figure 12a-c provides a direct comparison between these various derived quantities with the uncertainties of both methods (Figure 10).

From Figure 12d it follows that the overall trend of the air change rates based on the velocity measurements is in line with the rate based on the hourly averaged absolute pressure differentials.

Figure 12c shows that the air change rate with the indirect method with absolute pressure differentials corresponds to the air changes rates obtained from the direct method taking into account the uncertainty range. Yet as mentioned above these air change rates overestimate the actual cavity ventilation. On the other hand, Figure 12b shows that the air change rates from the indirect method are in good agreement with the 40% reduced air change rates from the direct method within the uncertainty range. Yet these air change rates correspond to an underestimation of the actual air change rate. Based on this it should be concluded that the actual air change rate

lies between the air change rates following from the indirect method and the direct method. The first is around 5-40% lower than the latter. It can be concluded that the reduction factor of 5-40% proposed by Falk [23], which was only based on anemometer measurements, is within a reliable range.

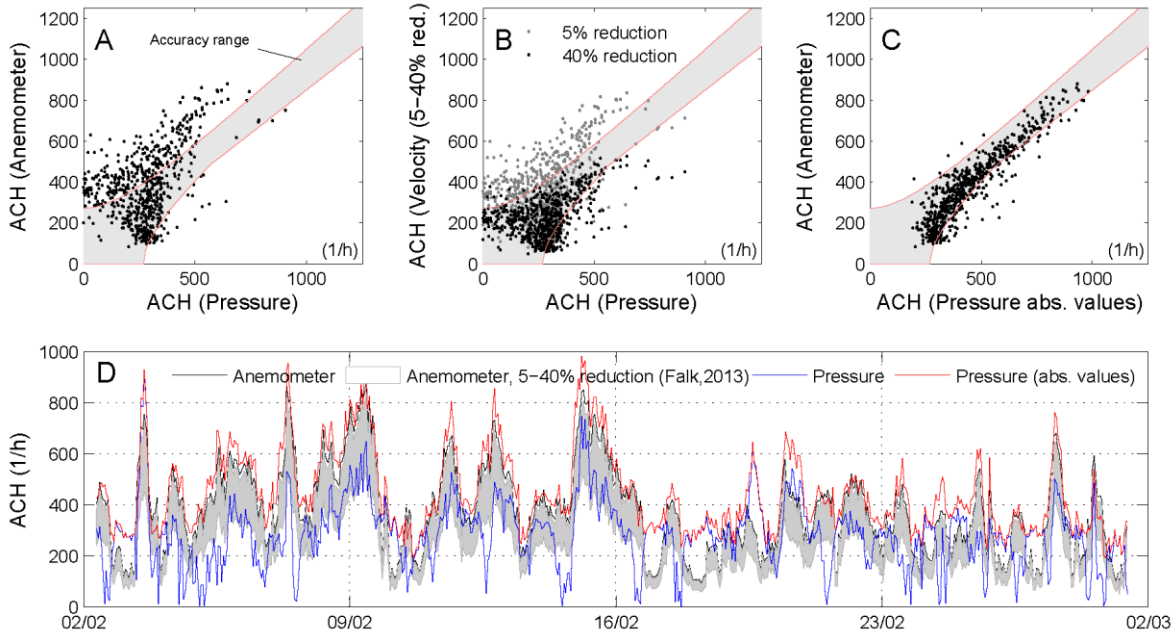

Figure 12: Comparison of air changes based on the direct and indirect measuring method for sidings system oriented to South West façade.

8. Temperature and relative humidity measurements

The continuous registration of the temperature and relative humidity can also bring insights in the air flow rates in the air cavity investigated. Figure 13 plots the relative humidity inside the Southwest and Northeast oriented test walls with brick veneer together with the outdoor relative humidity for the first two weeks of February. This graphs show that the averaged relative humidity is higher on the Southwest façade. As mentioned above this orientation corresponds to the prevailing wind-driven rain direction. This driving rain can be easily buffered within the capillary-active brick veneer. To illustrate this, Figure 13a gives the measured wind direction and speed and Figure 12c provides the rain precipitation on a horizontal surface. There seems no instant relation between the rain fall and the humidity in the air cavity. This is partly caused by the influence of the moisture capacity of the air which also is a function of the temperature.

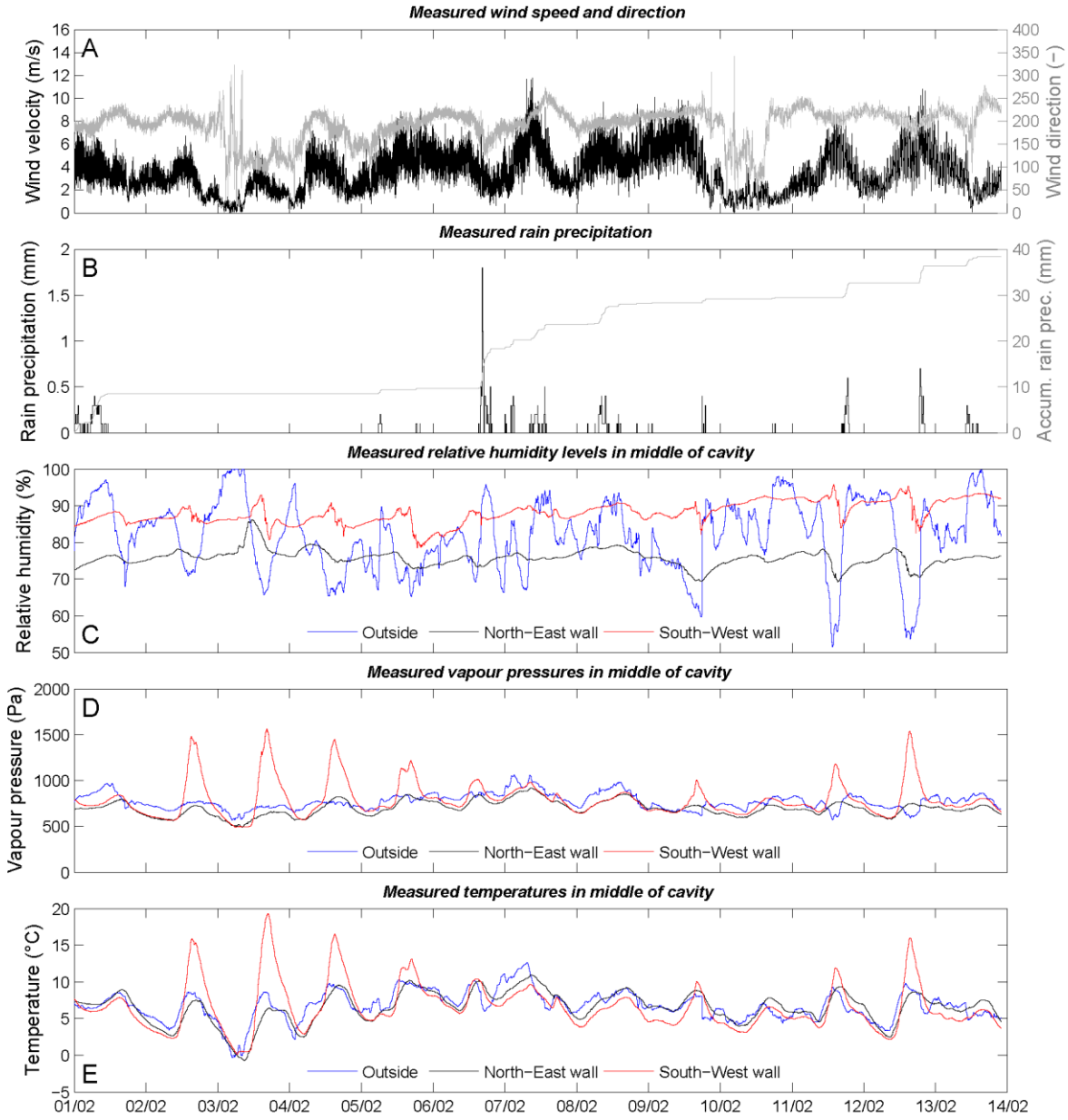

Figure 13: Brick veneer: Measured (A) wind speed and direction, (B) rain precipitation, (C) relative humidity in the in the middle of the cavities and the exterior climate, (D) vapour pressure in the middle of the cavities and the exterior climate, (E) temperature in the middle of the cavities and the exterior climate.

To tackle this issue Figure 13d provides the vapour pressures in the cavities which are calculated from the measured relative humidity ϑ (%) and temperature θ (°C) according to [38]:

$$P_v = \vartheta . \exp(65.8 - \frac{7066.3}{\theta} - 5.98 . \log(\theta)) \quad (12)$$

This graph reveals that the vapour pressure peaks simultaneously with the cavity's temperature on the Southwest façade (Figure 13e). This can be explained by solar driven vapour transport from the wet brick veneer to the cavity. Hereby the ventilation rate in the cavity is insufficient to remove this moisture flow completely, which explains the high peaks above the outdoor vapour pressure. When the solar radiation declines, this vapour flow

decreases and the cavity ventilation brings the cavity vapour pressure back to the level of the outdoor vapour pressure. This system can by modelled by a simple mass balance:

$$\frac{V}{R_v.T_{cav}}.\frac{\partial p_{v,cav}}{\partial t} = Q_v + Q_c = \left(p_{v,outside} - p_{v,cav}\right).\frac{ACH.V}{3600.R_v.T_{cav}} + \beta.A(p_{v,s} - p_{v,cav}) \quad (13)$$

which is illustrated in Figure 14 and in which Q_v (kg/s) is the vapour transported by ventilation, Q_c the convective vapour flux between brick veneer and air cavity (kg/s), V (m^3) the volume of the cavity (2.7x0.04x1 m^3), R_v (462 J/(kg K)) the gas constant of water vapour, T_{cav} (K) the cavity air temperature, A the brick veneer surface (2.7x1 m^2), β the mass transfer coefficient (s/m), p_v (Pa) the partial vapour pressure of air cavity/outside air and ACH (1/h) the air change rate per hour.

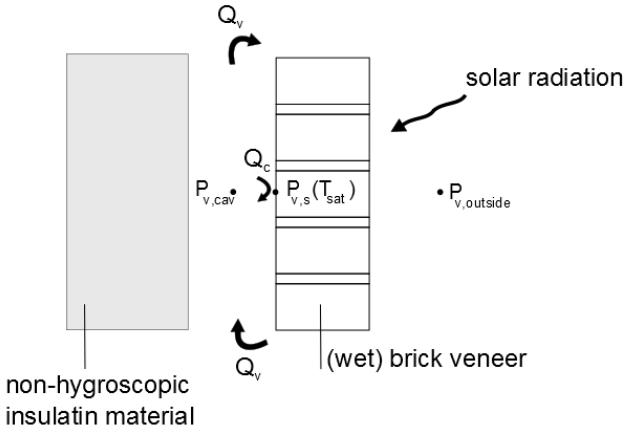

Figure 14: Schematical overview of vapour mass balance in air cavity.

This equation is solved for the first week of February with different assumed air change rates in the cavity. The results for three different constant air change rates (1, 10 and 100 1/h) and a varying air change rate based on the measured air pressure differentials are presented in Figure 15b together with the measured vapour pressure in cavity and the outdoor vapour pressure. The applied vapour transfer coefficient β is based on Janssens [39]:

$$\beta = \frac{Sh.\delta_a}{D/2} \quad (14)$$

in which δ_a is the vapour permeability in stagnant air (1.85 10^{-10} kg/s/m/Pa), Sh is the Sherwood number for convective mass transfer which is assumed 2 (-) (adopted from Janssens [39]) and D is the depth of the cavity (0.04 m). This results in a vapour transfer coefficient at the interface of the brick veneer layer and air cavity of 1.85 10^{-8} s/m. Further it is assumed that the vapour pressure at the surface of the brick veneer equals the saturation vapour pressure. This is a reasonable assumption because the sorption isotherm of brick veneer is typically quasi zero at low humidity levels and only starts to peak at humidty higher than 99%.

Figure 15b illustrates that the calculated vapour pressure based on the measured air change rate with the indirect method (blue) and the constant air change rate of 10 1/h (black) follow the measured vapour pressure in the cavity (red) most closely during the peaks. However, in periods with low solar radiation, which corresponds to lower vapour pressures, the uncertainty on the measured vapour pressure is too high to compare the different ACH-assumptions.

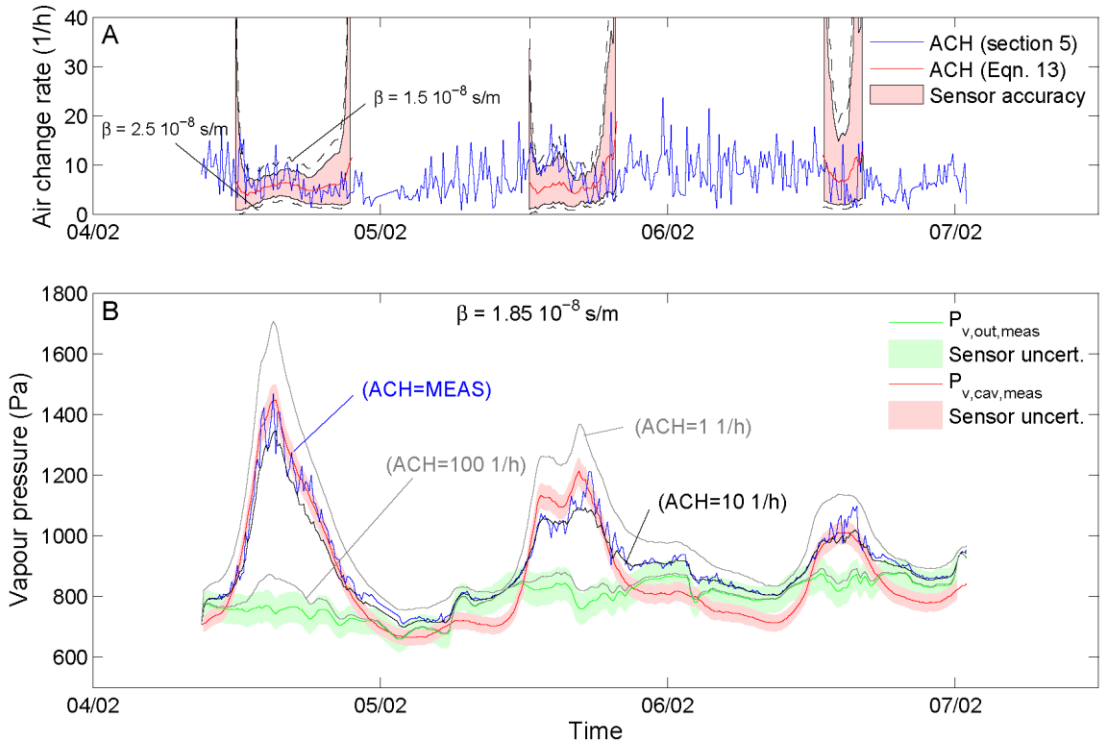

Figure 15: A) Comparison of the calculated ventilation rates based on Eqn. 13 and based on the indirect method for the first week of February 2014 B) comparison between measured vapour pressure in the air cavity (red), outside vapour pressure (green), simulated vapour pressure based with measured ventilation rate (blue) and constant ventilation rates (grey). (10-minute data).

In addition Eqn 13 is applied to derive the air change rate based on the measured vapour pressures. Figure 15a compares these results with the air change rate obtained from the indirect method (section 5). This figure includes the uncertainty related to the sensor accuracy. In addition, on the top of the sensor accuracy the vapour transfer coefficient is varied between 1.5 10^{-8} s/m and 2.5 10^{-8} s/m. The results indicate that the air change rate can only be predicted within a reasonbly accurcay range if the difference between the vapour pressure in the cavity and the outer vapour pressure is sufficiently high. Periods in which the accuarcy is more than 40 1/h are excluded from the graph. From Figure 15a it can be concluded that a good agreement between both methods is obained in periods in which the brick veneer layer is saturated in combination with high solar radiation peaks. In case one of these two criteria is missing the method based on the thermocouples and relative humidity sensors can not be used.

9. Discussion

The effectiveness of cavity ventilation may have a large impact on the hygrothermal behaviour of building constructions. Yet due to the complex nature of convective heat and moisture processes behind cladding systems, still significant uncertainties exist in today's measuring techniques to quantify cavity ventilation air change rates. The present article compared measuring methods in terms of applicability and reliability. In total four different measurement techniques to quantify the air change rate behind cladding systems have been verified based on full scale test walls exposed to exterior climate conditions.

Two tracer gas techniques have been applied: a) constant dosage and b) decay method. The results indicated that the first technique is not suitable to derive the air change rate on a continuous basis. The reasons are related to poor mixing of the tracer gas across the cavity and the low sampling frequency of these devices (typically around 10-15 minutes). Yet better results were obtained from the tracer gas decay method. Figure 3 illustrated that based on this procedure the air change rate for the brick veneer walls is between 2-3 ACH while the air change rate behind the siding was 100-1000 ACH for the same meteorological conditions. This is in line with the results of the other measuring techniques which will be shown below. However, it should be noted that in the present work a tracer gas with a high density (SF_6) was applied. At low ventilation rates (resulting in poor mixing) this influences the driving potentials and may thus bias the result. Therefore the authors recommend to apply a lighter tracer gas to avoid this influence.

The second measuring method deduced the air change rate indirectly from the measured pressure differentials by treating the ventilation cavity as ~~a~~ hydraulic network. The *in-situ* characterisation of the air resistance of the cavity by means of pressurisation testing indicated the importance of including the air permeability of the cladding material in the hydraulic model.

For the walls with sidings this method based on the measured pressure differentials could directly be compared with the data from the anemometers (direct method). The same trends were observed with both methods, however, the comparison revealed that the direct method overestimates the ventilation rate. The reason for this overestimation is related to the highly fluctuating air flow direction in the cavity related to variations in wind pressures. The indirect method based on the measured pressure differential is able to capture this effect. In contrast the omnidirectional anemometer did not register these changes in flow direction which can correspond to an overestimation during periods when a certain amount of air has not the time to exit the cavity before the direction changes. This was already addressed by Falk and Sandin [23] who proposed a reduction factor of 5-40%. Further analysis showed that this factor is in line with the measurements of the present study.

The direct method showed to be limited to cladding systems resulting in high air change rates. The applied anemometers for this method are typically installed from the inside, through the insulation layer. In winter conditions this results in a thermal bridge inducing local buoyant air flows around the sensors which may exceed the actual air velocities related to the cavity ventilation driven by the exterior climate. The study showed that this method is not applicable for brick veneer cladding which typically correspond to low ventilation rates (<10 ACH). Cladding systems with sidings, on the other hand, are typically more air open (100-1000 ACH), so, cavity ventilation airflow is overpowering this thermal bridge effect making this method applicable for these systems. However, for periods with low wind speeds and minimal buoyancy driven cavity flow, this thermal bridging effect may still be in the same order of magnitude of the actual ventilation rate. This means that even for air open systems, such as sidings, this thermal bridging effect may affect the results in periods with low air changes rates.

Finally a method was proposed to derived the air change rate behind brick veneer cladding based on the measured humidity conditions within the cavity and a simple mass balance. When brick veneer is saturated by rain and thereafter exposed to solar radiation moisture is driven into the cavity. This results in an increased vapour pressure depending on the moisture removal capacity which is related to the ventilation rate. The present study revealed that this method is only reliable for periods in which the difference between the outer vapour pressure and the vapour pressure behind the cladding systems is sufficiently high. Yet the results show that for periods in which this requirement is fulfilled, this method is in good agreement with the indirect method (<10ACH). The disadvantage of this method, however, is its limitation to capillary active cladding systems under saturated conditions.

10. Conclusions

The present article compares four different measuring techniques to quantify cavity ventilation rates on full scale test walls with brick veneer cladding and fibre cement sidings systems exposed to exterior conditions. In case of high ventilation rates (ACH > 100 ACH), the same trends were found for the methods based on direct velocity measurements with anemometers and the methods in which the air change rate is derived from the hydraulic network theory and measuring the pressure differentials across the cavity. The wall systems with sidings are relatively air open corresponding to air change rates in the range of 100-1000 ACH. As a result, good agreement between both methods was found for this cladding system. For the brick veneer cladding, on the other hand, the ventilation process is much slower (<10 ACH) and it was observed that the anemometer measurements were overpowered by local buoyancy effects induced by the measurements setup.

The methods based on the measured pressure differential show that wind induced cavity ventilation is highly unstable resulting in an air flow pattern frequently altering between upward and downward air flows. As a consequence the method based on the omnidirectional anemometers are overestimating the air change rates. A reduction factor of 5-40 % proposed by Falk and Sandin [23] were in line with the findings in the current study.

Furthermore, it was found that the conclusions from tracer gas method are limited to estimate the order of magnitude of the ventilation rate. Registrating the air change with high frequency in interaction with the climate conditions was not possible with this method.

Finally a method was proposed to derive the air change rate behind brick veneer based on the inward vapour transport driven by solar radiation. This low cost measuring method resulted in ventilation rate within the same order of magnitude as the results of the continuous pressure differentials measurements and tracer gas technique. However, its applicability is limited to capillary active cladding systems and to periods in which this layer is saturated and exposed to sufficient solar radiation.

Acknowledgements

Research funded by a Postdoctoral Innovation Mandate (grant number 140695) of the Institute for the Promotion of Innovation through Science and Technology in Flanders (IWT-Vlaanderen). In addition the support of Redco nv in this study is greatly acknowledged.

References

[1] Straube, J., (2012), High performance enclosures, Building Science Corporation.
[2] Davidovic, D., Srebric, J., & Burnett, E. F. P. (2006). Modeling convective drying of ventilated wall chambers in building enclosures. International Journal of Thermal Sciences, 45(2), 180–189.
[3] Gudum, C. (2003). Moisture Transport and Convection in Building Envelopes. Department of Civil Engineering, Technical University of Denmark.
[4] Salonvaara, M. H., Ojanen, T. T., Kokko, E., & Karagiozis, A. (1998). Drying Capabilities of Wood Frame Walls with Wood Siding. In Thermal envelope VII.
[5] Schumacher C., Shi X., Davidovic D., Burnett E., Straube J., Ventilation drying in wall systems in: Second International Building Physics Conference, Leuven, Belgium, September 14–18, 2003.
[6] Mao, Q., Fazio, P., & Rao, J. (2009). In-cavity evaporation allowance-A drying capacity indicator for wood-frame wall system. Building and Environment, 44(12), 2418–2429.
[7] Falk, J., & Sandin, K. (2013). Ventilated rainscreen cladding : A study of the ventilation drying process. Building and Environment, 60, 173–184. doi:10.1016/j.buildenv.2012.11.015
[8] Straube J., & Finch, G. (2009). Report 0906: Ventilated wall claddings: review, field performance, and hygrothermal modeling. test (p. 25). Waterloo. Retrieved from www.buildingscience.com
[9] Karagiozis, A., & Künzel, H. (2009). The Effect of Air Cavity Convection on the Wetting and Drying Behavior of Wood-Frame Walls Using a Multi-Physics Approach. Journal of ASTM International, 6(10)
[10] Salonvaara, M. H., Ojanen, T. T., Kokko, E., & Karagiozis, A. (1998). Drying Capabilities of Wood Frame Walls with Wood Siding. In Thermal envelope VII.
[11] Falk, J., Molnár, M., & Larsson, O. (2014). Investigation of a simple approach to predict rainscreen wall ventilation rates for hygrothermal simulation purposes. Building and Environment.
[12] Künzel, H. M., Karagiozis, A. N., & Kehrer, M. (2008). Assessing the benefits of cavity ventilation by hygrothermal simulation. In Building physics symposium in honour of Prof.Hugo L.S.C Hens. Leuven, Belgium.

[13] Salonvaara, M., Karagiozis, A., Pazera, M., & Miller, W. (2007). Air Cavities Behind Claddings - What Have We Learned? In Thermal Performance of the Exterior Envelope of Buildings X Conference. Clearwater, USA.
[14] Nore, K., Blocken, B., & Thue, J. V. (2010). On CFD simulation of wind-induced airflow in narrow ventilated façade cavities: Coupled and decoupled simulations and modelling limitations. Building and Environment, 45(8), 1834–1846.
[15] Stovall, T. K., & Karagiozis, A. (2004). Airflow in the Ventilation Space Behind a Rain Screen Wall. In Thermal Performance of the Exterior Envelope of Buildings IX Conference.
[16] Labat, M., Woloszyn, M., Garnier, G., Rusaouen, G., & Roux, J. J. (2012). Impact of direct solar irradiance on heat transfer behind an open-jointed ventilated cladding: Experimental and numerical investigations. Solar Energy, 86(9), 2549–2560.
[17] Falk, J., Molnár, M., & Larsson, O. (2014). Investigation of a simple approach to predict rainscreen wall ventilation rates for hygrothermal simulation purposes. Building and Environment. doi:10.1016/j.buildenv.2013.11.025
[18] Davidovic, D., Piñon, J., Burnett, E. F. P., & Srebric, J. (2012). Analytical procedures for estimating airflow rates in ventilated, screened wall systems (VSWS). Building and Environment, 47, 126–137.
[19] Straube, J., & Finch, G. (2009). Report 0906: Ventilated wall claddings: review, field performance, and hygrothermal modeling. test (p. 25). Waterloo.
[20] Nore, K. (2009). Hygrothermal performance of ventilated wooden cladding. Building. Norwegian University of science and technology, Norway.
[21] Bassett, M., & McNeil, S. (2009). Ventilating wall cavities above windows. Journal of Building Physics, 32(4), 305–318.
[22] TenWolde, A., Carll, C. and Malinauskas, V. (1995). Airflows and Moisture Conditions in Walls of Manufactured Homes, ASTM. STP 1255: Airflow Performance of Building Envelopes, Components and Systems, American Society for Testing and Materials, Philadelphia
[23] Falk, J., & Sandin, K. (2013). Ventilated rainscreen cladding : Measurements of cavity air velocities , estimation of air change rates and evaluation of driving forces. Building and Environment, 59, 164–176.
[24] Sandin K. Skalmurskonstruktionens fuktoch temperaturbetingelser, R43:1991, Technical University College, Lund [in Swedish].
[25] Desta, T. Z., Langmans, J., & Roels, S. (2011). Experimental data set for validation of heat, air and moisture transport models of building envelopes. Building and Environment, 46(5), 1038–1046.
[26] Blocken B, Carmeliet J. (2005). High-resolution wind-driven-rain measurements on a low-rise building - experimental data for model development and model validation. Journal of Wind Engineering and Industrial Aerodynamics 93(12): 905-928.
[27] Roels, S., & Deurinck, M. (2011). The effect of a reflective underlay on the global thermal behaviour of pitched roofs. Building and Environment, 46(1), 134–143
[28] Bejan, A. (2004). Convection heat transfer (Vol. Third). John Wiley & Sons, New Jersey, USA.
[29] Lecompte, J. (1989). The influence of natural convection on the thermal quality of insulated cavity walls constructions (in Dutch). KU Leuven, Laboratorium Bouwfysica, Heverlee.
[30] Kohonen, R. (1984). Transient analysis of the thermal and moisture physical behaviour of building constructions. Building and Environment, 19(1), 1–11.
[31] Idelchik IE. Handbook of hydraulic resistance. 3rd ed. CRC Press Inc.; 1994. [15] ASHRAE. Handbook of fundamentals. American Society of Heating, Refriger- ating and Airconditioning Engineers; 2009.
[32] Kronvall, J. (1980). Air flows in building components. Lund institute of technology, Sweden.
[33] Straube, J.F. and Burnett, E.F.P., (1998)"Vents, Ventilation and Masonry Veneer Wall Systems", Proc of the Eighth Canadian Masonry Symposium, Jasper, Alta., Canada, pp.194-207.
[34] Hens, H. (2006). The vapor diffusion resistance and air permeance of masonry and roofing systems. Building and Environment, 41(6), 745–755.
[35] Langmans, J., Klein, R., De Paepe, M., & Roels, S. (2010). Potential of wind barriers to assure airtightness of wood-frame low energy constructions. Energy and Buildings, 42(12), 2376–2385.
[36] Liddament, M. W. (1996). A guide to energy efficient ventilation. (A. infiltration and V. C. International Energy Agency, Ed.). U.K.: Oscar Faber Partnership.
[37] www.halstrup-walcher.de/en/produkte/alle_produkte/P-26.php
[38] Hens (2012) Building Physics -Heat, Air and Moisture: Fundamentals and Engineering Methods with Examples and Exercises, ISBN: 978-3-433-60130-3
[39] Janssens, A. (1998). Reliable control of interstitial condensation in lightweight roof systems: calculation and assessement methods. Ph.D. thesis, KU Leuven, Laboratorium Bouwfysica, Heverlee.